

RESEARCH

Open Access



Outer membrane vesicles of *Porphyromonas gingivalis* impede bone regeneration by inducing ferroptosis via the Hippo-YAP signaling pathway

Xinghong Luo^{1†}, Yanzhen Wang^{2†}, Tingting Ning^{1†}, Qian Lei¹, Hao Cui², Xianghui Zou², Yan Chen³, Shuoling Chen², Xinyao Zhang², Shenglong Tan¹ and Dandan Ma^{1*}

Abstract

Background Although increasing evidence confirms that oral microbiota imbalance is a critical factor inhibiting bone regeneration, the specific mechanisms have remained unexplored. This study aims to use periodontitis as a model of oral microbiota imbalance to investigate the specific mechanisms that inhibit bone regeneration in extraction sockets.

Methods Cone Beam Computed Tomography (CBCT) data of extraction sockets were collected from patients with and without periodontitis to confirm the influence of the periodontitis microenvironment on bone regeneration in extraction sockets. Furthermore, GW4869-pretreated *Porphyromonas gingivalis* (Pg) and normal Pg were used to build a periodontitis model, and then the bone regeneration in extraction sockets under these conditions was detected by H&E staining, Masson's staining and micro-CT analysis. In vitro, the effect of Pg-derived OMVs on osteogenic differentiation of bone marrow mesenchymal stem cells (BMSCs) was examined. RNA sequencing, FerroOrange, malondialdehyde assay, transmission electron microscopy, qRT-PCR, and western blotting analysis were performed.

Results CBCT analysis showed that periodontitis significantly inhibited new bone formation in the extraction sockets in patients. Micro-CT and Histological analysis revealed that inhibiting OMVs released from Pg alleviated the inhibition of bone regeneration in extraction sockets under Pg imbalance. Moreover, Pg-derived OMVs treatment deteriorated bone regeneration in extraction sockets. In vitro, results showed that Pg-derived OMVs inhibited osteogenic differentiation of BMSCs. Furthermore, the results indicated a significant upregulation of ferroptosis in OMVs-treated BMSCs. Notably, targeting ferroptosis promoted osteogenic differentiation of BMSCs and bone regeneration in extraction sockets, as compared with the OMVs-treated group. Mechanistic studies have shown that Pg-derived OMVs promoted BMSCs ferroptosis via the Hippo-Yes-associated protein (YAP) pathway.

Conclusion This study shows that a Pg microbiota imbalance inhibits bone regeneration by secreting OMVs from Pg to induce ferroptosis in BMSCs. Mechanically, we illustrated that OMVs induce ferroptosis through the Hippo-YAP

[†]Xinghong Luo, Yanzhen Wang and Tingting Ning have contributed equally to this work.

*Correspondence:

Dandan Ma
mdd@smu.edu.cn

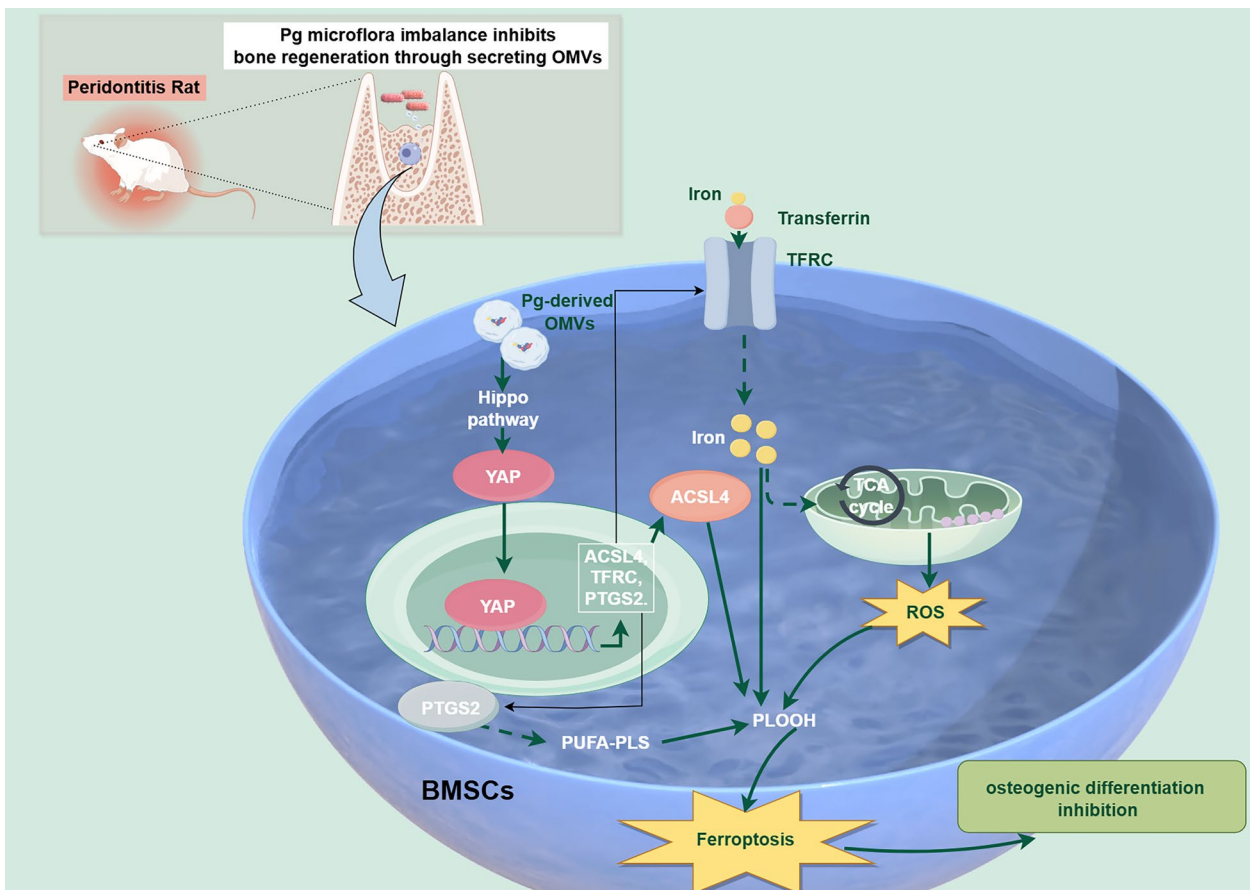
Full list of author information is available at the end of the article



pathway. These findings might provide a new insight and potential therapeutic target to promote bone regeneration under oral microbiota imbalance.

Keywords Oral microbiota imbalance, OMVs, BMSCs, Bone regeneration, Ferroptosis

Graphical Abstract



Introduction

The oral microbiome is composed of over 700 different bacterial strains, and in a healthy state, the interactions within the oral microbiota and between it and the host are in a state of dynamic equilibrium [1]. Previous studies have shown that there is no difference in the composition of the oral microbiota patients without periodontitis and those with periodontitis; the main difference lies in the significantly increased proportion of periodontitis pathogens, such as *Porphyromonas gingivalis* (Pg), within the oral microbiota [2]. This suggests that the occurrence of the disease is not only due to the specific pathogenic bacteria but is also promoted by microbial imbalance. In recent years, the

impact of oral microbiota imbalance on bone homeostasis and bone regeneration has become a focus of attention [3, 4]. However, the regulatory mechanisms of oral microbiota imbalance on bone regeneration still need to be further elucidated. Periodontitis is a typical disease caused by an imbalance of pathogens such as Pg [2, 5]. Therefore, using periodontitis as a research model to explore the impact and specific mechanisms of Pg microbiota imbalance on bone regeneration will help clarify the mechanisms by which oral microbiota imbalance affects bone regeneration and provide new insights.

Bacterial outer membrane vesicles (OMVs) are nanovesicles of 20–350 nm, secreted by Gram-negative bacteria [6, 7]. Studies have reported that OMVs are one of

the critical regulators that mediate the development of diseases by carrying molecules [8, 9]. Recently, OMVs have been a regulator of bone formation and osteoclast formation. OMVs from child gut microbiota can promote bone formation and inhibit bone loss [10]. Besides, *Proteus mirabilis* OMVs were reported to inhibit osteoclast formation and bone loss by inducing mitochondrial apoptosis through the miR96-5p/abca1 signaling axis [9]. However, *Filifactor alocis* OMVs, derived from periodontitis microbiota, can increase the expression levels of pro-inflammatory cytokines and promote osteoclast formation via Toll-like receptors, resulting in systemic bone loss [11]. Moreover, *Fusobacterium nucleatum* OMVs could promote osteoclastic differentiation and alveolar bone loss in periodontitis [12, 13]. The above studies show that OMVs have dual roles in bone homeostasis, and their function mainly depends on the origination and the contents they carried. Pg microbiota imbalance is the leading pathogenic cause of periodontitis, and its OMVs were associated with many diseases [5, 14, 15]. Researchers have shown the role of Pg OMVs in osteoclast formation and inflammation during alveolar bone resorption under periodontitis [14]. Still, the role in osteogenic formation and bone regeneration has not yet been reported. Whether the dysbiosis of periodontitis microbiota in the microenvironment affects the process of bone regeneration through the secretion of OMVs by Pg still needs further investigation.

Ferroptosis is induced by iron-dependent lipid peroxidation [16]. The biological characteristics of ferroptosis are unique, such as intercellular iron overload, decreasing glutathione peroxidase 4 (GPX4) expression, and increased lipid peroxidation [17, 18]. Ferroptosis also exhibits mitochondrial vacuolization and the mitochondrial ridge decreases or disappears [17]. Moreover, prostaglandin-endoperoxide synthase 2 (PTGS2) and acyl-CoA synthetase long chain member 4 (ACSL4) are the mediators that promote lipid peroxidation, and both are essential regulator of ferroptosis [19–21]. Accumulating evidence has confirmed that ferroptosis is closely related to osteoporosis, cancer therapy, and neurodegeneration [22–24]. Therefore, targeting ferroptosis is a potential treatment strategy. A recent study has indicated that high-dose dexamethasone promoted osteoporosis by inducing ferroptosis in osteoblasts by downregulating GPX4 [25]. High glucose inhibited MC3T3-E1 cells' osteoblastic differentiation by ferroptosis [26, 27]. Besides, targeting ferroptosis can rescue osteocyte death and trabecular deterioration in diabetic osteoporosis [22]. These previous studies suggest that ferroptosis may be an effective regulator of osteogenic formation and bone homeostasis. However, whether OMVs can mediate ferroptosis has yet to be elucidated.

In this study, we found the crucial role of Pg OMVs in suppressing osteoblastic differentiation of bone marrow mesenchymal stem cells (BMSCs) and limiting bone regeneration under Pg microbiota imbalance. Mechanistically, we confirmed that Pg OMVs inhibited the osteoblastic differentiation of BMSCs by inducing ferroptosis via the Hippo- Yes-associated protein (YAP) pathway. Furthermore, targeting ferroptosis significantly rescued the poor bone regeneration of extraction sockets caused by Pg OMVs. Our research will provide insight into the underlying mechanism of poor bone regeneration under dysregulation of periodontitis microflora and provide a potential therapeutic target for bone regeneration.

Methods

Cone Beam Computed Tomography (CBCT) data collection

The human ethics approval of this study was approved by Ethics Committee of Stomatological Hospital of Southern Medical University (Approved number NYKQ-EC-[2024]07). CBCT data of molar extraction sockets was collected from aged 25–45 years old non-periodontitis and periodontitis patients at the Maxillofacial Surgery Department of Stomatology Hospital of Southern Medical University, and patients provided their informed consent. The CBCT data were included immediately and 3 months after extraction and further analyzed the extraction sockets by YlzRtBrowser and ITK-SNAP software for buccal alveolar ridge height (BARH), lingual alveolar ridge height (LARH), Alveolar ridge width (ARW) and new bone formation.

Animals

The ethics protocol of the animal research in this study has received the ethical approval from Nanfang Hospital Animal Ethic Committee of Southern Medical University (Approved number IACUC-LAC-20230218-001). Male Sprague Dawley (SD) rats of 4–6 weeks were purchased from the Guangdong Province Animal Center. Rats were housed under conditions with a temperature of 22 ± 2 °C, a 12-h light/dark cycle, and provided with free access to a regular diet and water. Rats were anesthetized with 1.5% isoflurane, and then a 3-0 silk ligature was fastened around the bilateral maxillary second molar to establish an experimental periodontitis model. 100 μ L 10^8 /mL Pg were injected into the periodontal pocket every other day for 2 weeks. The first molar of the bilateral mandibular was extracted after the periodontitis model was successfully established. Rats were euthanatized at 7 and 14 days to collect the mandibular and maxillary samples. Besides, to evaluate the effect of OMVs on bone regeneration of extraction sockets, rats were anesthetized with 1.5% isoflurane and then the first molar of the bilateral mandibular was extracted. An equal volume of

phosphate-buffered saline (PBS) or 10 µg Pg OMVs was injected into the extraction sockets every other day. Rats were euthanized at 7 and 14 days to collect the mandibular and maxillary samples for further experiments.

According to the manufacturer's instructions (Beyotime, China), Pg was labeled with DiO dye. Then, the 10^7 labeled Pg were injected into the periodontal pocket every other day for 2 weeks, followed by collecting the gingival crevicular fluid (GCF) and saliva from normal rats and periodontitis mice induced by DiO-labeled Pg. The collected fluid was subsequently centrifuged at $8000\times g$ for 20 min, followed by additional centrifugation at $10,000\times g$ for 30 min at 4 °C. The fluid was then passed through a 0.22-µm filter. Further purification of OMVs was achieved by subjecting the filtrate to ultracentrifugation at $150,000\times g$ for 150 min at 4 °C. Then, flow cytometry was used to determine the concentration of Pg-derived OMVs with green fluorescence in the GCF and saliva.

Micro-CT

Samples were maintained in 4% paraformaldehyde solution at a temperature of 4 °C for 24 h, followed by imaging through micro-CT scanning (Scanco Medical, AG, Switzerland) with a resolution of 12-µm. The data was reconstructed, and bone volume/total volume (BV/TV), trabecular thickness (Tb. N) and trabecular number (Tb. Th) of the molar extraction sockets were measured and analyzed by supporting software.

Histological analyzed

Immunofluorescence and histochemical staining with hematoxylin and eosin (H&E) were performed. Briefly, rat specimens were fixed in 4% paraformaldehyde fixation for 48 h, decalcified up to 4 weeks in 10% ethylenediaminetetraacetic acid, and embedded in paraffin wax. The embedded specimens were subsequently cut into sections of 4-µm-thick, which were then subjected to Masson's staining and H&E staining procedures. For the immunofluorescence assay, the sections were treated with antibodies specific to the following protein: STRO-1 (Novus, USA), PTGS2 (Abmart, China), and YAP (Abmart, China).

Cell culture and identification

BMSCs were isolated from the bone marrow of SD rats. In brief, the femur of rats was meticulously flushed to obtain bone marrow cells that subsequently collected. The collected cells then cultured in alpha-minimum essential medium (MEM) (Gibco) enriched with 10% fetal bovine serum (FBS) (Gibco) and incubated at 37 °C under 5% CO₂ overnight. Following incubation, the non-adherent cells were removed by washing with PBS. Flow

cytometric analysis was applied to identify the surface immunophenotypic markers of BMSCs. BMSCs were incubated with cluster of differentiation (CD) 29 antibody, CD45 antibody and CD90 antibody. The osteoblastic differentiation of BMSCs was induced using a specialized differentiated medium, which included 50 µg/mL ascorbic acid and 10 mM β-glycerol phosphate. The adipogenic differentiation of BMSCs was induced with the adipogenic medium (Pythonbio, China).

MC3T3-E1 cells were obtained from the Cell Bank of the Chinese Academy of Science. MC3T3-E1 cells were cultured in alpha-MEM (Gibco) enriched with 10% FBS (Gibco) and incubated at 37 °C under 5% CO₂. The differentiation medium of MC3T3-E1 cells contained 50 µg/mL ascorbic acid and 10 mM β-glycerol phosphate.

Bacterial culture and OMVs preparation

Pg Strain ATCC33277 was purchased from the Guangdong Microbial Culture Center. Pg were cultured in brain–heart infusion (BHI) both supplemented with vitamin K (1 µg/mL), hemin (5 µg/mL) and 5% defibrinated sheep blood in an anaerobic chamber. Upon reaching the late exponential phase, the culture medium of Pg was harvested, and the medium was subsequently centrifuged at $8000\times g$ for 20 min, followed by an additional centrifugation at $10,000\times g$ for 30 min at 4 °C. The medium was then passed through a 0.22-µm filter. Further purification of OMVs was achieved by subjecting the filtrate to ultracentrifugation at $150,000\times g$ for 150 min at 4 °C.

The particle size and morphology of the OMVs were evaluated by Nanoparticle tracking analysis (NTA) and transmission electron microscopy, respectively.

Inhibition of Pg OMVs secretion

GW4869 was used to inhibit the Pg OMVs secretion as in the previous studies [8, 10]. Briefly, Pg was cultivated in a complete growth medium supplemented with 10 µM GW4869 (MedChemEpress, USA), or an equivalent volume of the vehicle (DMSO), within an incubator set at 37 °C and maintained under anaerobic condition. 2 days later, remove the stimulant and Pg was continued to grow in a fresh complete medium. The viability of Pg was evaluated by bacterial proliferation assay. The conditioned media were collected to isolate the Pg OMVs to assess the sustained inhibitory effects of GW4869 on the release of Pg OMVs. The protein concentration and particle count of the isolated Pg OMVs were evaluated by the BCA Protein Assay Kit and NTA, respectively.

OMVs uptake by BMSCs in vitro

0.4 µL of PKH67 dye was used to mark 10 µg OMVs for 2 min. To remove the excess unbound dye, the mixture underwent ultracentrifugation at $150,000\times g$ at

4 °C for 150 min. Following centrifugation, the OMVs were carefully pelleted and resuspended in PBS for further use. Subsequently, BMSCs were co-cultured with PKH67-labeled OMVs at 10 µg/mL concentration, maintained at 37 °C with 5% CO₂ for 12 h. Following this incubation period, the cells were fixed using 4% paraformaldehyde and then the cell nuclei were dyed with DAPI (Abcam, UK). The internalization of the OMVs was visualized utilizing fluorescence microscopy (Olympus, Japan). Besides, BMSCs were co-cultured with PKH67-labeled OMVs at 10 µg/mL concentration, BMSCs were co-cultured with PKH67-labeled OMVs at 10 µg/mL concentration, maintained at 37 °C with 5% CO₂ for 12 h. Following this incubation period, the cells were washed and resuspended in PBS, then analyzed using a flow cytometer (Beckman DxFLUO, USA).

CCK8 assays

CCK8 assays was carried out following the previously described method [28].

qRT-PCR

qRT-PCR analysis was carried out following the previously described method [28]. The sequences of the primers in this study are displayed in Table 1. The 2^{-ΔΔCT} method was used to calculate the relative expression of the target genes.

Table 1 Primers used for qRT-PCR

Target gene	Primer sequence
GAPDH	Forward: GACATGCCGCTGGAGAAAC Reverse: AGCCCAGGATGCCCTTAGT
ALP	Forward: CACGGCGTCCATGAGCAGAAC Reverse: CAGGCACAGTGGTCAAGGTTGG
RUNX2	Forward: TTCAACGATCTGAGATTTGTGGG Reverse: GGATGAGGAATGCGCCCTA
OCN	Forward: GGACCTCTCTGCTCACTCTG Reverse: ACCTTACTGCCCTCCTGCTTGG
BMP2	Forward: AAGCGTCAAGCCAAACACAAACAG Reverse: CCAGTCATTCCACCCACATCAC
PTGS2	Forward: AGGTCATCGGTGGAGAGGTGTATC Reverse: CGGCACCAGACCAAGACTTCC
ACSL4	Forward: CCATATCGCTGTGACGCACTTC Reverse: CCAGGCTGCTCTTCCCAAAC
TFRC	Forward: GTTCCCGTTGTTGAGGCAGAC Reverse: GATGACTGAGATGGCGGAAACTGAG
GPX4	Forward: CCAGCAACAGCCACGAGTTCC Reverse: CACACGCAACCCCTGTACTTATCC

Western blotting

The specific procedures of western blotting analysis were carried out as previously described [28]. The following primary antibodies were used: alkaline phosphatase (ALP) (Abmart, China), osteocalcin (OCN) (Abmart, China), bone morphogenetic protein 2 (BMP2) (Abmart, China), YAP (Abmart, China), p-YAP (Abmart, China), Glyceraldehyde-3-phosphate dehydrogenase (GAPDH) (Proteintech, China), GPX4 (Abmart, China), ACSL4 (Abmart, China), PTGS2 (Abmart, China), Transferrin Receptor 1 (TFRC) (Abmart, China) and Histone H3.1 (Abmart, China).

Alizarin Red S staining and ALP staining

ALP staining, Alizarin Red S staining, and the quantification of Alizarin Red S staining were carried out as detailed in previous study [28].

Oil Red O staining

Oil Red O staining was carried out as detailed in previous study [28].

Fe²⁺ measurement

FerroOrange was used to detect intracellular divalent iron ions in strict adherence to the protocol provided by the manufacturer (DOJINDO, Japan). After treatment, BMSCs were incubated with FerroOrange (DOJINDO, Japan) at temperature of a 37 °C with 5% CO₂ for 30 min. Then, cells were labeled with Hoechst 33258 (Beyotime, China) to mark the cell nuclei. The cells were observed by confocal microscope (Leica STELLARIS 5, Germany).

Transmission electron microscopy (TEM)

The changes in mitochondrial morphology were detected by TEM. After treatment, BMSCs were centrifuged at 800×g for 3 min after trypsinization and fixed for 24 h at 4 °C. Then, cells were dehydrated, embedded, sectioned, stained, and observed by JEM-1400Plus TEM.

Malondialdehyde (MDA) assay

The level of MDA was determined by MDA Assay Kit (Beyotime, China). After treatment, cells were detected by the MDA Assay kit according to the manufacturer's instructions. The samples were measured the absorbance at 532 nm.

RNA sequencing

BMSCs were co-cultured with 10 µg/mL OMVs or vehicle in 6-well plates. Following the co-culture period, the total RNA was isolated from the cells. The isolated total RNA was then processed to purify mRNA using magnetic beads conjugated with poly-Toligo. Next, the Cluster Profiler R package was then used to identify the

significantly enriched Kyoto Encyclopedia of Gene and Genomes (KEGG) pathway.

Chromatin immunoprecipitation (ChIP) qPCR

A ChIP Assay Kit (Beyotime, China) was used for ChIP analysis of YAP and PTGS2, ASCL4 or TFRC promotor interaction. In brief, cells treated with 10 $\mu\text{g}/\text{mL}$ OMVs were fixed with 1% formaldehyde, lysed and homogenized using a Dounce homogenizer. DNA was shorn by sonication, and the sheared chromatin was incubated with 2 mg of IgG (Sigma-Aldrich, USA) or YAP antibody (1:100; Abmart, China), followed by qPCR using the following primers:

PTGS2-F: GCCAAGAACGTACGGTTTAATTG
 PTGS2-R: TTCCCATAACTGGCCTTATTC
 ASCL4-F: AAACCCTGAAAGTCTCTGCTC
 ASCL4-R: TACAATTGCTCGCCTCAGATT
 TFRC-F: CACGCCTTTATTCCTACCACTC
 TFRC-R: CTAAGTCTGGACCCCTTTACAC

Statistical analysis

Statistical analysis was performed using GraphPad Prism software (San Diego, USA). Unpaired t-tests

were performed for group comparisons. All data were presented as mean values \pm SEM, with the provision for significance set at $p < 0.05$, in most cases based on the collection of at least three independent samples.

Results

Periodontitis inhibits bone regeneration after tooth extraction in patients

To confirm the role of periodontitis in bone regeneration of extraction sockets, we collected the CBCT data immediately and 3 months after extraction of non-periodontitis and periodontitis patients both without system diseases. Analysis of the BARH and LARH showed that, compared with non-periodontitis, periodontitis markedly increased the decrease of BARH and LARH, which indicated that periodontitis increased horizontal bone loss (Fig. 1A, B). As shown in Fig. 1C, analysis of the ARW indicated that periodontitis obviously increased the decrease of ARW. Besides, the new bone formation in extraction sockets was significantly inhibited by periodontitis patients (Fig. 1D, E).

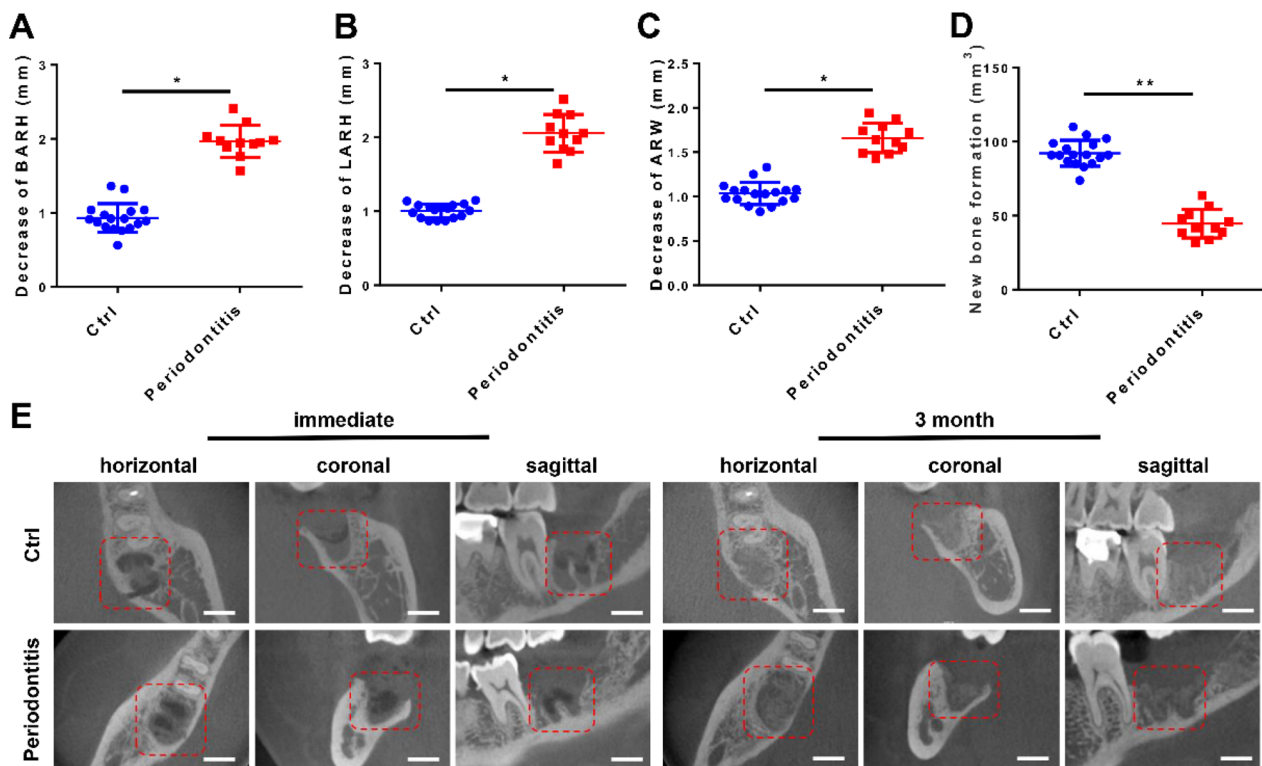


Fig. 1 Periodontitis inhibits bone regeneration after tooth extraction in patients. **A–C** CBCT data of patients with or without periodontitis were collected, and decreases in BARH (**A**), LARH (**B**), and ARW (**C**) were increased in periodontitis patients ($n = 11$), as compared with the healthy control group ($n = 17$). **D** CBCT data quantitative analysis showed that the new bone formation was significantly inhibited in periodontitis group ($n = 11$), as compared with the healthy control group ($n = 17$). **E** CBCT representative images showed that periodontitis patients had significantly worse new bone formation in extraction sockets than the control group ($n = 11$) (scale bar = 0.5 cm)

Inhibiting Pg secreting OMVs rescues bone regeneration in Pg microbiota imbalance

Pg microbiota imbalance is the leading pathogenic cause of periodontitis, and OMVs release is one of the most vital pathways of Pg interacting with the host. To confirm the presence of OMVs of Pg in the periodontitis model, Pg was labeled with DiO green, which is a fluorescent dye. The labeled Pg were injected into the periodontal pocket every other day for 2 weeks, then OMVs were collected from the GCF and saliva from normal rats and periodontitis mice induced by DiO-labeled Pg. The flow cytometry results showed that the proportion of Pg-derived OMVs in the GCF and saliva in the periodontitis model was about 17.2%, indicating the presence of Pg-derived OMVs in the periodontitis model (Supplementary Fig. 1A, B). To investigate whether Pg microbiota imbalance inhibits bone regeneration through the secretion of OMVs, GW4869 was used to pretreat Pg to inhibit Pg secreting OMVs. The proliferation results showed that GW4869 did not significantly affect the growth ability of Pg (Fig. 2A). BCA analysis showed that the protein contents of OMVs in Pg were notably reduced by GW4869 (Fig. 2B). NTA analysis indicated that the particle number of OMVs was remarkably decreased in the medium after being treated with GW4869 (Fig. 2C). These results confirmed the significant inhibition of GW4869 on OMVs release. To investigate whether the effects of periodontitis microenvironment on bone regeneration of extraction sockets depend on Pg-derived OMVs, we treated rat extraction sockets with GW4869-pretreated Pg (to inhibit OMVs secreting) and the schematic diagram of the animal experiment was presented in Fig. 2D. The micro-CT analysis indicated that the BV/TV, Tb.N, and Tb.Th of the extraction sockets were significantly decreased after Pg treatment, but the decrease was reversed by inhibiting Pg releasing OMVs (Fig. 2E, F). H&E staining showed a great decrease in bone formation in extraction sockets after Pg treatment, but inhibiting Pg-derived OMVs release can reduce the decrease of bone formation (Fig. 2G). Masson staining revealed a significant decrease in collagen fiber deposition after Pg treatment, but the decrease of the collagen fiber deposition in the extraction sockets was reversed by inhibiting Pg releasing OMVs (Fig. 2H). These results suggested that Pg-derived OMVs may be important in bone regeneration.

Pg-derived OMVs inhibit bone regeneration in vivo

Next, to further confirm the role of Pg-derived OMVs in bone regeneration, we isolated Pg-derived OMVs and characterized them using TEM and NTA. TEM and NTA analysis showed that Pg-derived OMVs displayed cup-shaped or spherical morphologies (Fig. 3A) and the mean

diameters of Pg-derived OMVs were 150.9 nm (Fig. 3B), similar to that previously reported OMVs from bacteria [8, 10, 29]. To further determine the role of Pg-derived in the bone regeneration of the extraction sockets, we injected OMVs into the extraction sockets. As shown in Fig. 3C, the schematic diagram of the animal experiment was presented. Micro-CT analysis indicated a notable decrease in BV/TV, Tb.N, and Tb.Th of the extraction sockets by Pg-derived OMVs (Fig. 3D–G). H&E staining showed that OMVs decreased trabecular bone formation (Fig. 3H). Masson staining revealed that collagen fiber deposition in the extraction sockets was notably reduced by Pg-derived OMVs (Fig. 3I).

Pg-derived OMVs inhibit osteogenic differentiation of BMSCs in vitro

BMSCs are important cells involved in bone regeneration, so we further investigated whether Pg-derived OMVs inhibiting the osteogenic differentiation of BMSCs in vitro. Firstly, primary BMSCs were successfully collected from rat femur and passaged. The isolated BMSCs were positive for CD29 and CD90 expression but negative for CD45 expression (Fig. 4A) and can form lipid droplets and mineralized nodules after being induced differentiation (Fig. 4B, C). As shown in Fig. 4D, PKH67 labeled Pg-derived OMVs were successfully taken up by BMSCs. Furthermore, the flow cytometry results showed that more than 99% of BMSCs have taken up the PKH67 labeled OMVs (Fig. 4E). Next, BMSCs were cocultured with 0 $\mu\text{g}/\text{mL}$, 0.1 $\mu\text{g}/\text{mL}$, 1 $\mu\text{g}/\text{mL}$, and 10 $\mu\text{g}/\text{mL}$ Pg-derived OMVs in the differentiated medium. The CCK8 assays analysis revealed that 0.1 $\mu\text{g}/\text{mL}$ and 1 $\mu\text{g}/\text{mL}$ Pg-derived OMVs did not inhibit the proliferation capacity of BMSCs, but 10 $\mu\text{g}/\text{mL}$ Pg-derived OMVs significantly inhibited the proliferation capacity of BMSCs (Supplementary Fig. 2). The qRT-PCR results revealed that ALP, OCN, RUNX2, and BMP2 expression levels were gradually down-regulated by Pg-derived OMVs, and 10 $\mu\text{g}/\text{mL}$ Pg-derived OMVs significantly decreased ALP, OCN, RUNX2, and BMP2 expression (Fig. 4F). The findings of the western blotting experiment revealed a gradual decrease in the expressions of ALP, OCN, and BMP2 by Pg-derived OMVs (Fig. 4G, H; Supplementary Fig. 3). The increasing concentration of Pg-derived OMVs successively reduced ALP activity and the mineralized nodule formation (Fig. 4I, J).

The effect of Pg-derived OMVs on the osteogenesis of MC3T3-E1 cells has also been evaluated. BMSCs were cocultured with 0 $\mu\text{g}/\text{mL}$ or 10 $\mu\text{g}/\text{mL}$ Pg-derived OMVs in the differentiated medium. The qRT-PCR results revealed that ALP, OCN, and BMP2 expression levels were significantly decreased by Pg-derived OMVs (Supplementary Fig. 4A). The findings of the western

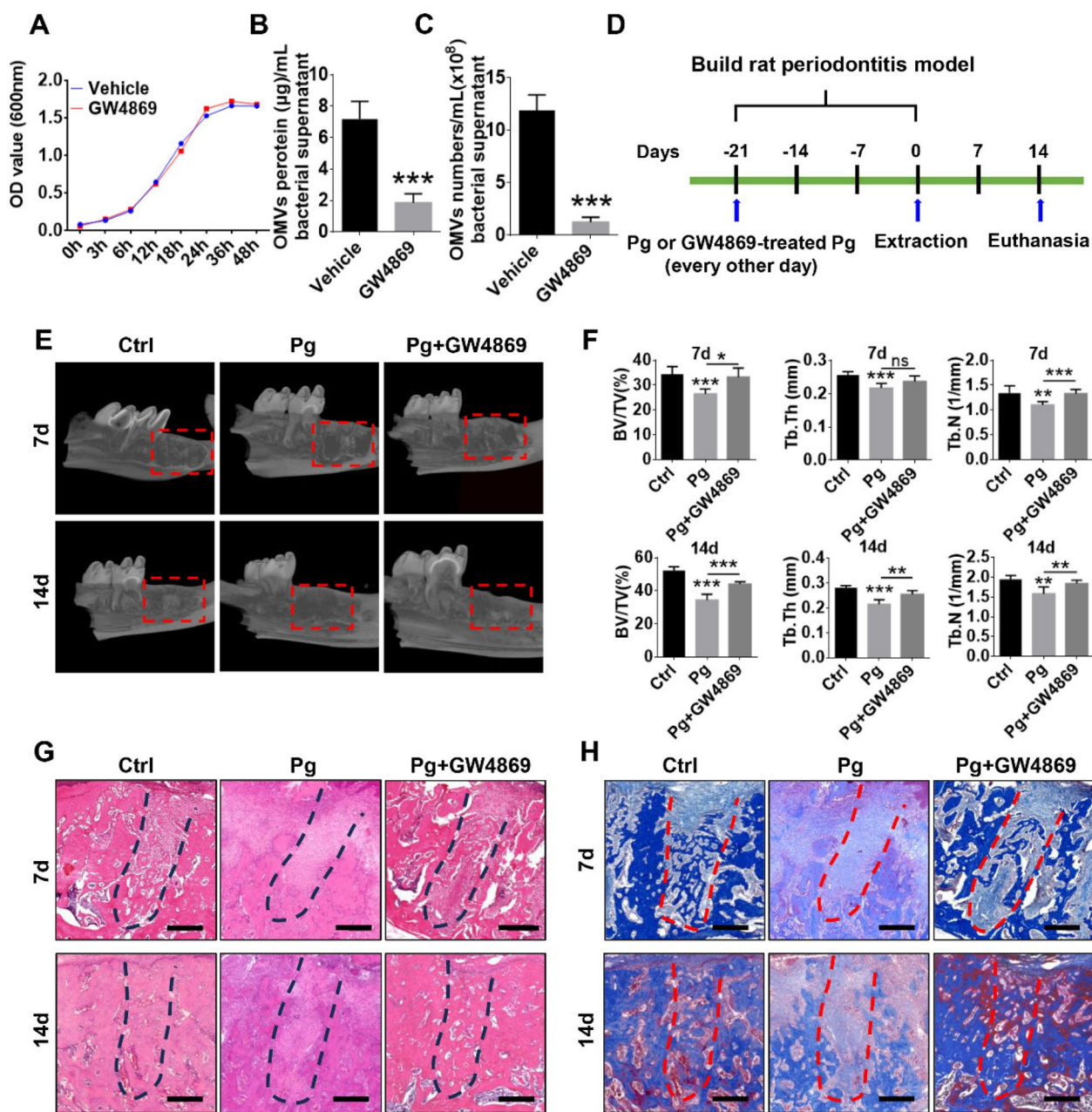


Fig. 2 Inhibiting Pg secreting OMVs rescues bone regeneration in Pg microbiota imbalance. **A** The growth curve of Pg under vehicle and GW4869 treatment. **B** BCA analysis showed that the protein contents of OMVs were reduced by GW4869. **C** NTA analysis indicated that the particle number of OMVs decreased remarkably in the medium after being treated with GW4869. **D** A schematic illustration of tooth extraction under periodontitis microenvironment model established by Pg or GW4869-treated Pg. **E** Representative micro-CT images of extraction sockets in the control group, Pg group and GW4869-treated Pg Group. **F** The bone regeneration of the extraction sockets was determined by micro-CT analysis of BV/TV, Tb.N, and Tb.Th (control group: n = 6, Pg group: n = 6, GW4869-treated Pg Group: n = 6). **G** The new bone formation was determined by H&E staining (scale bar = 400 µm). **H** The collagen fiber deposition was evaluated by Masson staining of extraction sockets (scale bar = 400 µm)

(See figure on next page.)

Fig. 3 Pg-derived OMVs inhibits bone regeneration in vivo. **A** OMVs were isolated from Pg, and their morphological analysis was examined by TEM (scale bar = 200 nm). **B** The particle size of Pg-derived OMVs was detected by NTA analysis. **C** The schematic diagram of the animal experiment. **D** Representative micro-CT images of the extraction sockets in control group and OMVs group (scale bar = 2 mm). **E–G** Micro-CT analysis indicated a notable decrease in BV/TV, Tb.N, and Tb.Th of the extraction sockets by Pg-derived OMVs (control group: n = 6; OMVs group: n = 6). **H** The new bone formation of the extraction sockets was detected by H&E staining (scale bar = 400 µm). **I** The Masson staining results (scale bar = 400 µm)

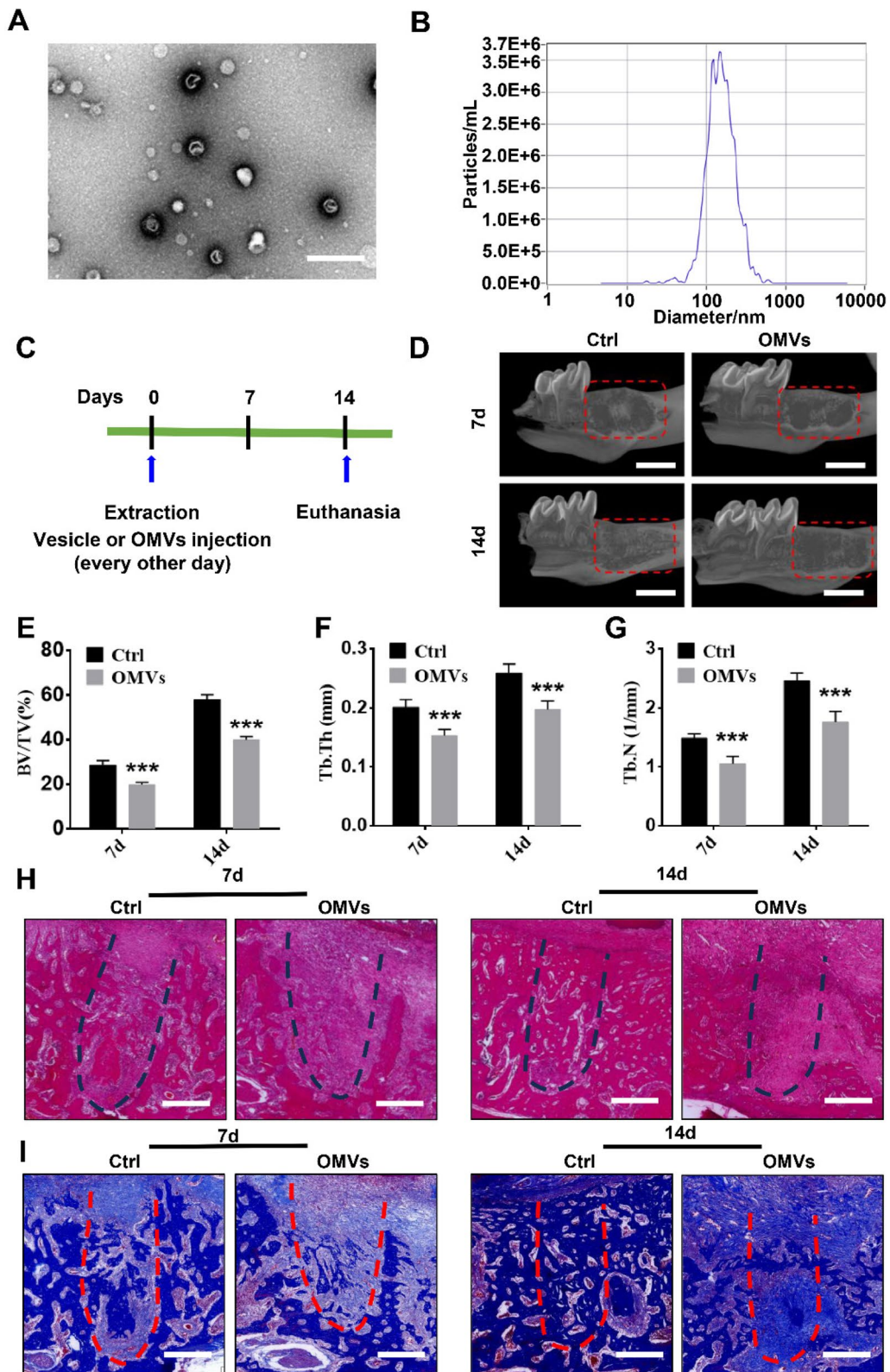


Fig. 3 (See legend on previous page.)

blotting experiment revealed an obvious decrease in the expressions of ALP, OCN, and BMP2 by Pg-derived OMVs (Supplementary Fig. 4B). Besides, ALP activity and the mineralized nodule formation were significantly reduced by Pg-derived OMVs (Supplementary Fig. 4C, D).

Pg-derived OMVs activate ferroptosis in BMSCs

RNA sequencing was performed to gain further insight into the underlying mechanism of Pg-derived OMVs inhibiting BMSCs osteogenic differentiation. The RNA sequencing analysis identified a total of 2682 differentially expressed genes ($p < 0.05$ and $|\log_2\text{fold-change}| > 1$), including 1535 down-regulated and 1147 up-regulated genes (Fig. 5A). Furthermore, results of KEGG pathway enrichment analysis results ($p < 0.05$) showed that the ferroptosis pathway was markedly up-regulated in the OMVs-treated BMSCs (Fig. 5B). qRT-PCR analysis was performed and revealed that the ferroptosis markers (ACSL4, TFRC, and PTGS2) expression levels were dramatically increased, and the inhibitor of ferroptosis (GPX4) was significantly decreased (Fig. 5C). The western blotting results also displayed similar results in protein expression levels (Fig. 5D, E; Supplementary Fig. 5). We further examined the ferroptosis-related morphological and biochemical changes. Transmission electron microscopy showed that mitochondria were deformed after Pg-derived OMVs treatment (Fig. 5F). Besides, BMSCs were cocultured with PKH67-labeled Pg-derived OMVs and detected using FerroOrange staining. The results showed iron overload in Pg-derived OMVs treated cells (Fig. 5G). MDA assay results indicated that malondialdehyde was significantly increased after Pg-derived OMVs treatment (Fig. 5H). Furthermore, immunofluorescence colocalization results showed that, in Pg-derived OMVs treated extraction socket, the expression of PTSG2 was dramatically increased in stro-1 positive BMSCs in vivo (Fig. 5I). These results confirmed that Pg-derived OMVs can induce ferroptosis in BMSCs. Given the above results, we speculated that ferroptosis

may be essential for Pg-derived inhibiting osteogenic differentiation of BMSCs.

Inhibiting ferroptosis reverses the negative effect of Pg-derived OMVs on osteogenic differentiation of BMSCs

Ferostatin-1 (Fer-1) has been confirmed to be an effective inhibitor of ferroptosis [30]. To verify the above hypothesis, we used Fer-1 to inhibit ferroptosis and observed whether Fer-1 could rescue the negative effect of Pg-derived OMVs on the osteogenic differentiation of BMSCs. The OMVs-induced increase of intracellular iron overloading was strongly blocked by Fer-1 (Fig. 6A). TEM results showed that Pg-derived OMVs caused mitochondrial vacuolation and deformation, which appeared to be rescued by Fer-1 (Fig. 6B). Further, increases in intracellular MDA production due to Pg-derived OMVs were largely blocked by Fer-1 (Fig. 6C). The western blotting results displayed that Fer-1 treatment partially restored the expression levels of the ferroptosis markers (ACSL4, TFRC, and GPX4) (Supplementary Fig. 6). These results indicated that Fer-1 successfully inhibited ferroptosis. qRT-PCR analysis showed that the mRNA expression levels of ALP, OCN, and BMP2 were significantly inhibited by Pg-derived OMVs; however, the OMVs-induced decrease was markedly rescued by Fer-1 (Fig. 6D). Similarly, Pg-derived OMVs inhibited the expression of ALP, OCN, and BMP2 protein expression but were reversed by Fer-1 (Fig. 6E, F; Supplementary Fig. 7). Furthermore, mineralized nodule formation was decreased by Pg-derived OMVs, but reversed upon inhibiting Ferroptosis (Fig. 6G, H). ALP activity staining revealed an obviously decline in osteogenic differentiation capacity when BMSCs were cocultured with Pg-derived OMVs, but decline tendency was reversed by Fer-1 (Fig. 6I).

Inhibiting ferroptosis promotes the bone regeneration

To investigate whether inhibiting ferroptosis could rescue the negative effect of Pg-derived OMVs on bone regeneration, we injected the Fer-1 into extraction sockets while OMVs injection, the samples were collected for assessment on 7 days and 14 days after treatment. Micro-CT analysis showed that BV/TV and Tb.N were decreased by

(See figure on next page.)

Fig. 4 Pg-derived OMVs inhibit osteoblastic differentiation of BMSCs in vitro. **A** The flow cytometry results of CD29, CD90 and CD45 in the isolated BMSCs. **B** Oil Red O staining results (scale bar = 200 μm). **C** Alizarin Red S staining results (scale bar = 200 μm). **D** Most BMSCs displayed strong intracellular green fluorescence which indicated that Pg-derived OMVs successfully entered BMSCs. Nucleus have been labeled with DAPI (blue), actin filaments have been labeled with DY-554 phalloidin (red), and OMVs have been labeled with PKH67 (green). The bottom white lines represented the scale bar (scale bar = 50 μm). **E** Flow cytometry result showed the proportion of BMSCs taken up the PKH67 labeled OMVs. **F** qRT-PCR analysis of ALP, OCN, RUNX2, and BMP2. **G, H** ALP, OCN, and BMP2 protein expression levels were determined by western blotting. Full-length blots are displayed in supplementary Fig. 3. **I** ALP activity was detected by ALP staining (scale bar = 250 μm). **J** Alizarin Red S staining results (scale bar = 250 μm)

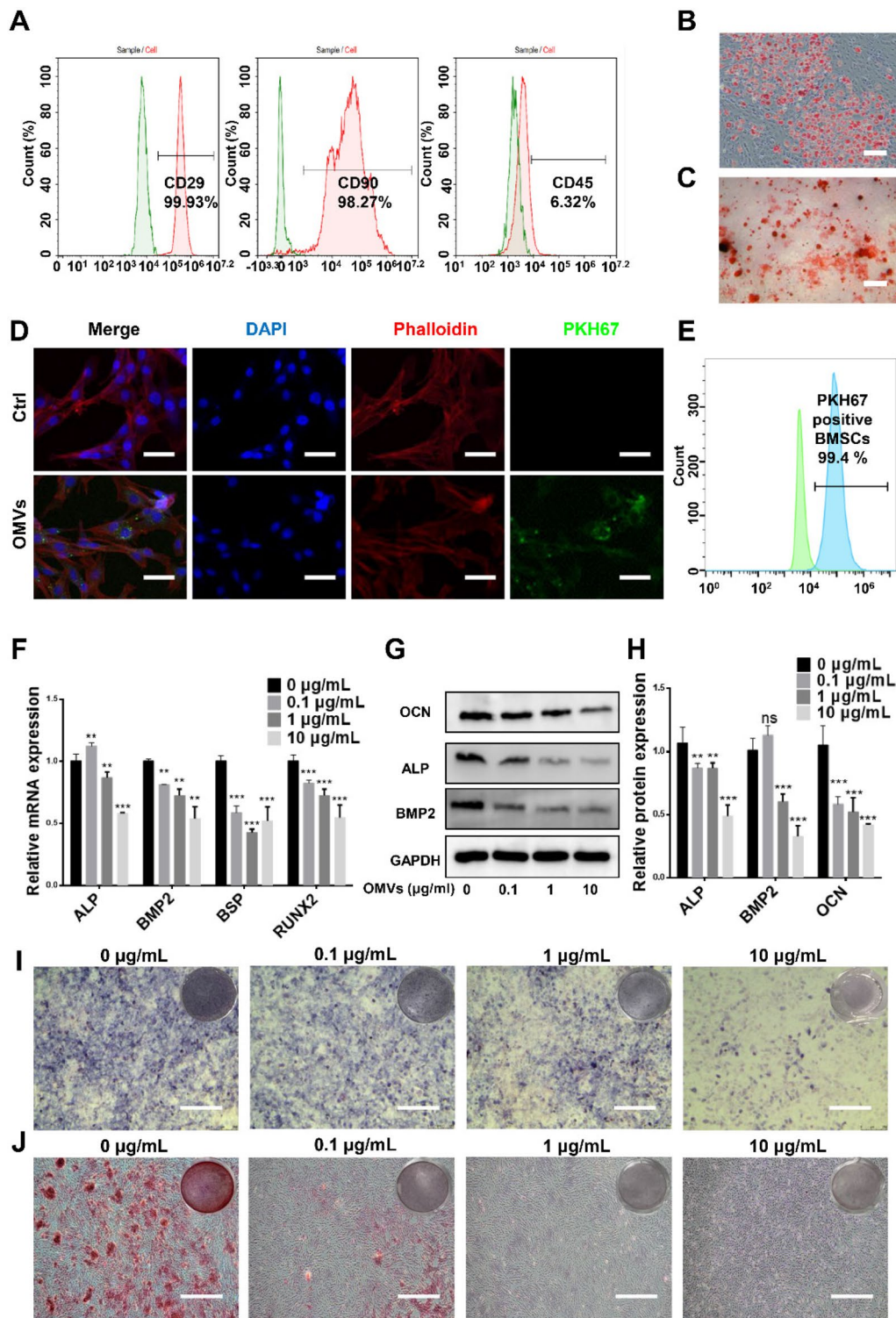


Fig. 4 (See legend on previous page.)

Pg-derived OMVs, but the decline tendency was almost reversed by Fer-1 (Fig. 7A–C). In addition, H&E staining showed that Fer-1 could promote bone formation

of extraction sockets, which was inhibited by OMVs (Fig. 7D). As shown in Fig. 7E, Masson staining revealed a significant decrease in the collagen fiber deposition in

the extraction sockets in OMVs group, but Fer-1 treatment improved the collagen fiber deposition in the extraction sockets as compared with OMVs group. Thus, the in vitro and in vivo results of inhibition of ferroptosis suggested its essential role in OMVs inhibiting bone regeneration in extraction sockets. However, the mechanism of Pg-derived OMVs regulating BMSCs ferroptosis remains unknown.

Pg-derived OMVs regulate BMSCs ferroptosis via the Hippo-YAP pathway

The sequencing analysis showed that Pg-derived OMVs markedly upregulated genes involved in ferroptosis, including ACSL4, TFRC, and PTGS2 (Fig. 8A), which has been confirmed in the above results. To explore the mechanism of Pg-derived OMVs regulating BMSCs ferroptosis, we used the TF-Target Finder to predict and find the possible upstream transcription factor of ACSL4, TFRC, and PTGS2, respectively (based on the ChIP Atlas and GTRD database). Then, the Venn diagram was used to identify the common upstream transcription of prediction transcription factors, and the results revealed that YAP was the common upstream transcription factor of ACSL4, TFRC and PTGS2 (Fig. 8B). Interestingly, KEGG pathway enrichment analysis ($p < 0.05$) showed that the Hippo signaling pathway was significantly down-regulated in the Pg-derived treated cells (Fig. 8C). It's well known that YAP is the critical transcription factor of the Hippo signaling pathway; when this pathway is inhibited, then YAP translocates to the nucleus to stimulate target genes transcription [31]. Studies have shown that YAP could promote the transcription of ACSL4, TFRC and PTGS2 [32, 33]. In this study, the ChIP-qPCR analysis showed that YAP could bind the promoter regions of ACSL4, TFRC and PTGS2 genes (Supplementary Fig. 8). Thus, we speculated that Pg-derived OMVs might regulate ferroptosis in BMSCs through YAP. The immunofluorescence results showed that YAP levels significantly increased in the nucleus after OMVs treatment (Fig. 8D). Western blotting results indicated that YAP was strongly up-regulated in the nucleus, while p-YAP was significantly decreased in the cytoplasm after OMVs treatment (Fig. 8E, F; Supplementary Fig. 9A-D).

The immunofluorescence results showed that YAP levels significantly increased in the nucleus in stro-1 positive BMSCs in the OMVs treated alveolar sockets (Fig. 8G). Then, we used Verteporfin (YAP inhibitor) to inhibit the expression of YAP. From western blotting analysis, YAP expression was down-regulated clearly in the nucleus by Verteporfin (Fig. 8H; Supplementary Fig. 9E, F). TFRC, ACSL4, and PTGS2 expressions were all significantly increased with Pg-derived OMVs, but reversed by YAP inhibitor, as evidenced by qRT-PCR and western blotting (Fig. 8I, J; Supplementary Fig. 9G-J). These results demonstrated that Pg-derived OMVs promoted ferroptosis in BMSCs via the Hippo-YAP signaling pathway (Fig. 9).

Discussion

Although increasing evidence confirms that oral microbiota imbalance is a critical factor inhibiting bone regeneration, the specific mechanisms must be adequately elucidated. This study found that Pg microbiota imbalance inhibits bone regeneration in extraction sockets by secreting OMVs from Pg. We demonstrated that Pg-derived OMVs inhibited bone regeneration by inducing BMSCs ferroptosis. Notably, targeting ferroptosis promoted osteogenic differentiation of BMSCs and bone regeneration in extraction sockets. Mechanically, we confirmed that Pg-derived OMVs promoted BMSCs ferroptosis via the Hippo-YAP pathway.

Oral microbial homeostasis is closely related to bone homeostasis and regeneration [34]. To explain the influence the oral microbiome has on alveolar bone homeostasis in health and disease, a new term was proposed by Chen et al. "oral osteomicrobiology" [35]. It's well known that periodontitis is a disease caused by oral microbial imbalance, and an imbalance of Pg is the leading cause of periodontitis [5]. In this study, we used Pg to construct dysregulation of periodontitis microflora and investigate bone regeneration under Pg microbiota imbalance. Micro-CT analysis, H&E staining, and Masson staining results showed that bone regeneration in the extraction sockets was significantly inhibited by periodontitis, which was consistent with findings in previous studies [36, 37]. However, the underlying mechanism still needs to be further explored. Oral microorganisms interact

(See figure on next page.)

Fig. 5 Pg-derived OMVs activate ferroptosis in BMSCs. **A** RNA sequence analysis of differentially expressed genes displayed in volcano plot. **B** KEGG pathway enrichment analysis between the control group and OMVs group. **C** The ACSL4, TFRC, PTGS2, and GPX4 expression levels were measured by qRT-PCR. **D** Western blotting results of ACSL4, TFRC, PTGS2, and GPX4, Full-length blots are displayed in supplementary Fig. 5. **E** Quantitative results of western blotting. **F** Transmission electron microscopy showed that mitochondria were deformed after Pg-derived OMVs treatment (scale bar = 500 nm). **G** Results of FerroOrange staining showed that Iron overload in Pg-derived OMVs treated cells (scale bar = 50 μ m). **H** MDA assay results indicated that malondialdehyde was significantly increased after Pg-derived OMVs treatment. **I** immunofluorescence colocalization results showed that, in Pg-derived OMVs treated extraction socket, the expression of PTGS2 was dramatically increased in stro-1 positive BMSCs in vivo (scale bar = 50 μ m)

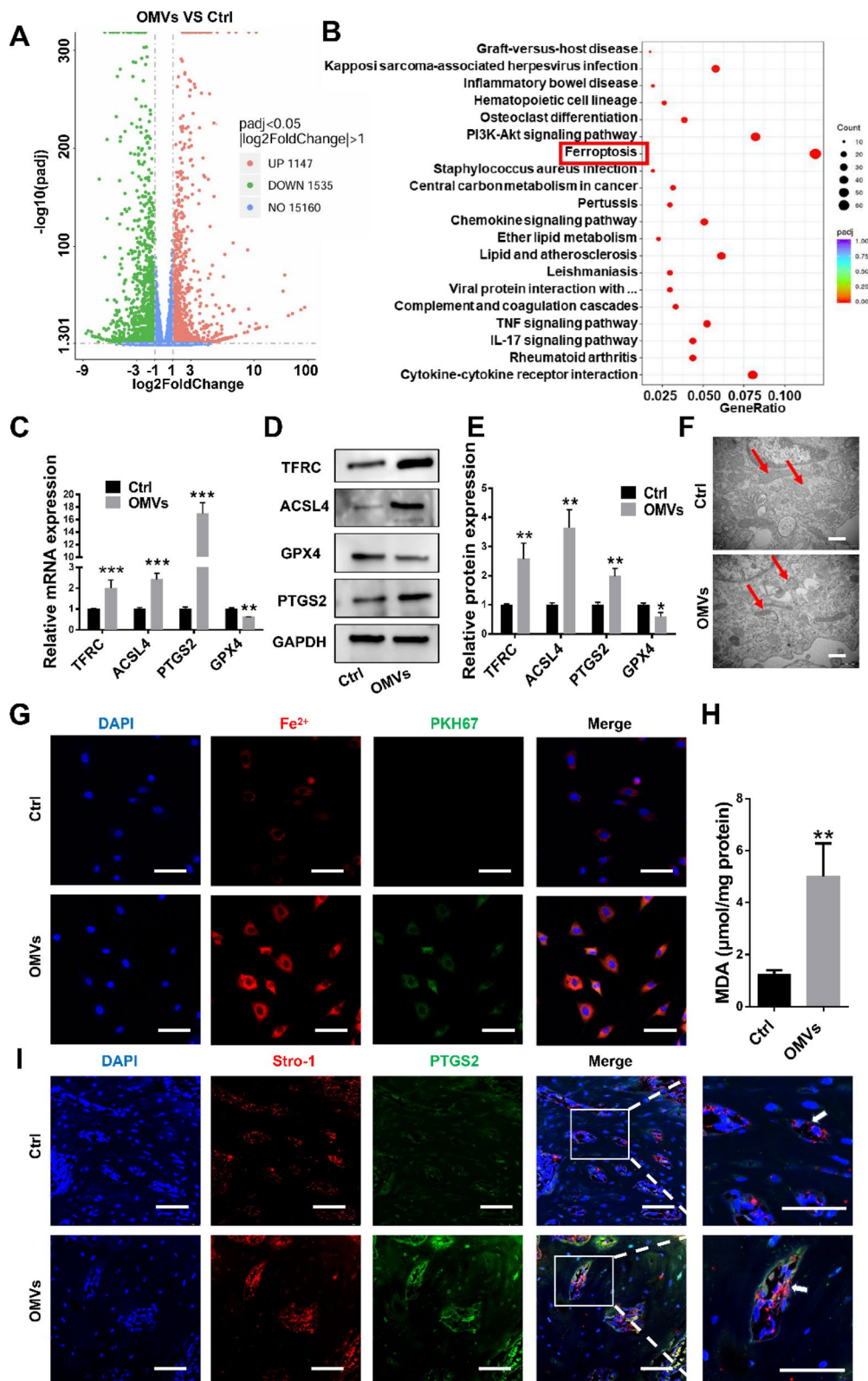


Fig. 5 (See legend on previous page.)

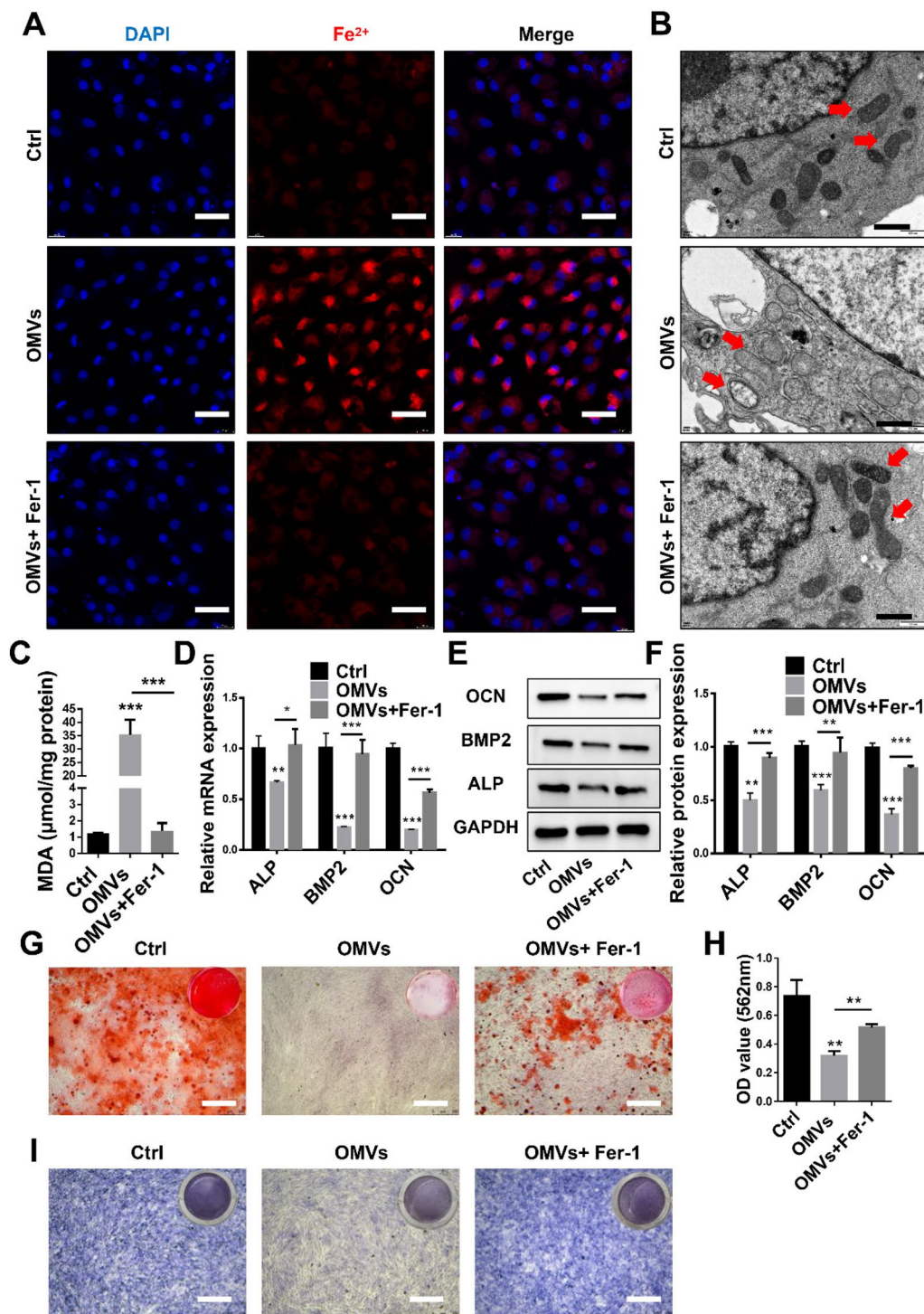


Fig. 6 Inhibiting ferroptosis reverses the negative effect of Pg-derived OMVs on osteogenic differentiation of BMSCs. **A** FerroOrange staining revealed that the OMVs-induced increase in intracellular iron overloading was strongly blocked by Fer-1 (scale bar=40 μm). **B** TEM results revealed that Pg-derived OMVs caused mitochondrial vacuolation and deformation, but mitochondrial vacuolation and deformation can be rescued by Fer-1 (scale bar = 500 nm). **C** The results of MDA assay. **D** qRT-PCR analysis of ALP, OCN, and BMP2. **E, F** Western blotting results of ALP, OCN, and BMP2. Full-length blots are displayed in supplementary Fig. 7. **G** Alizarin Red S staining results (scale bar = 250 μm). **H** The quantitative results of Alizarin Red S staining. **I** ALP activity staining results revealed the ALP activity of BMSCs was inhibited by Pg-derived OMVs, but the decline tendency was reversed by Fer-1 (scale bar = 250 μm)

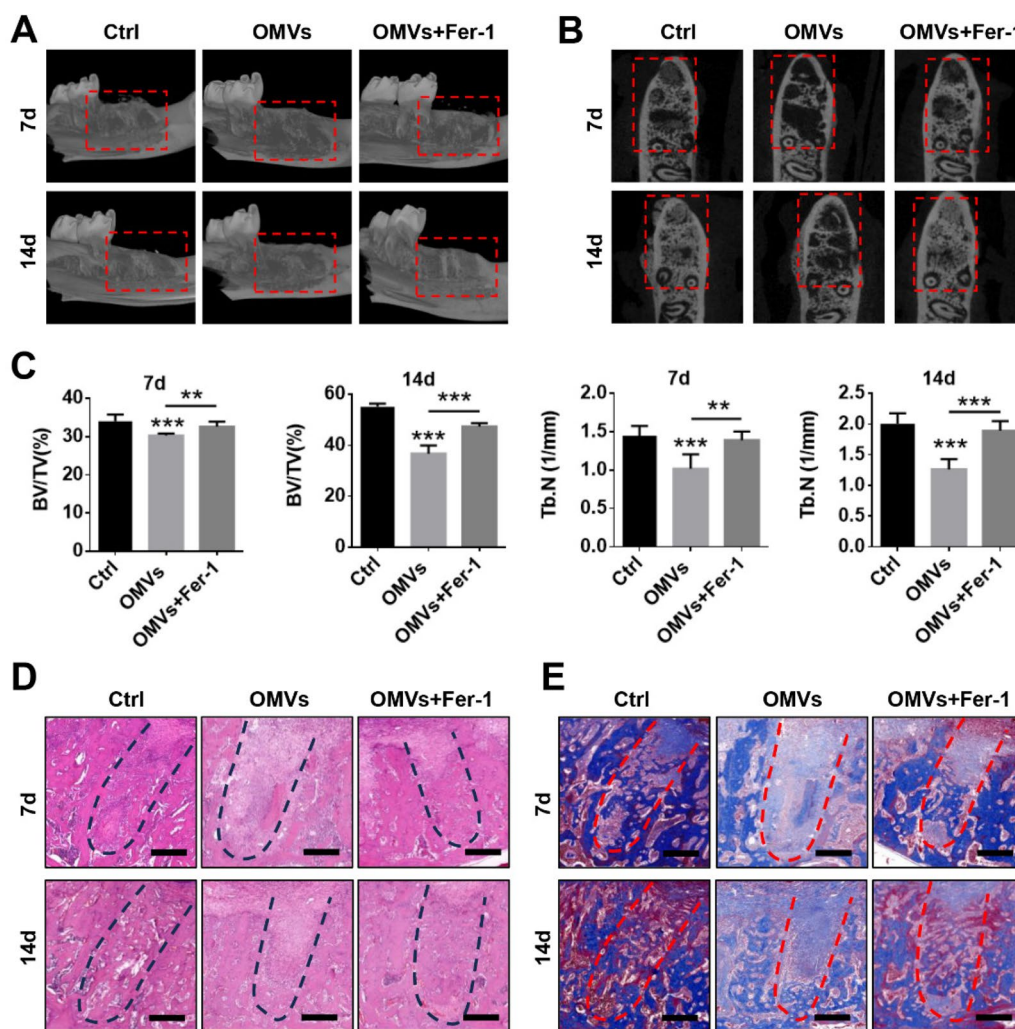


Fig. 7 Inhibiting ferroptosis promotes the bone regeneration. **A, B** Representative micro-CT images (scale bar = 2 mm). **C** Micro-CT analysis results of BV/TV, Tb.N, and Tb.Th. in the control group (n = 6), OMVs group (n = 6) and OMVs + Fer-1 group (n = 6). **D** H&E staining showed that Fer-1 could promote the bone formation of extraction sockets, which was inhibited by OMVs (scale bar = 400 μm). **E** Collagen fiber deposition observed by Masson staining (scale bar = 400 μm)

with the host with a complicated communication system, and OMVs are the primary communication messenger molecules [8]. In our study, we used GW4869 to inhibit the secretion of OMVs by Pg. BCA and NTA analysis confirmed that GW4869 successfully inhibited the secretion of OMVs by Pg. Previously, GW4869 was also used

to inhibit the secretion of OMVs by *Akkermansia muciniphila*, *Fusobacterium nucleatum*, and *Cyanobacterium* [8, 10, 38]. Our study showed that inhibiting the secretion of OMVs by Pg could reverse the adverse effect of the Pg microbiota imbalance on bone regeneration in extraction sockets. In addition, we used Pg-derived OMVs to

(See figure on next page.)

Fig. 8 Pg-derived OMVs regulate BMSCs ferroptosis via the Hippo-YAP pathway. **A** Heatmap of RNA-sequencing analysis. **B** TF-Target Finder was used to predict and find the possible upstream transcription factor of ACSL4, TFRC, and PTGS2, respectively (based on ChIP Atlas database and GTRD database). The Venn diagram showed the intersection of predicted transcription factors of ACSL4, TFRC, and PTGS2. **C** KEGG pathway enrichment analysis. **D** The immunofluorescence results of YAP in the nucleus (scale bar = 30 μm). **E, F** Western blotting results of YAP protein and p-YAP protein. **G** The immunofluorescence results of YAP and stro-1 in the sockets (scale bar = 50 μm). **H** Western blotting results of YAP expression in the nucleus. **I** qRT-PCR results of TFRC, ACSL4, and PTGS2. **J** The protein expression levels of TFRC, ACSL4, and PTGS2 were measured by western blotting. Full-length blots are presented in supplementary Fig. 9

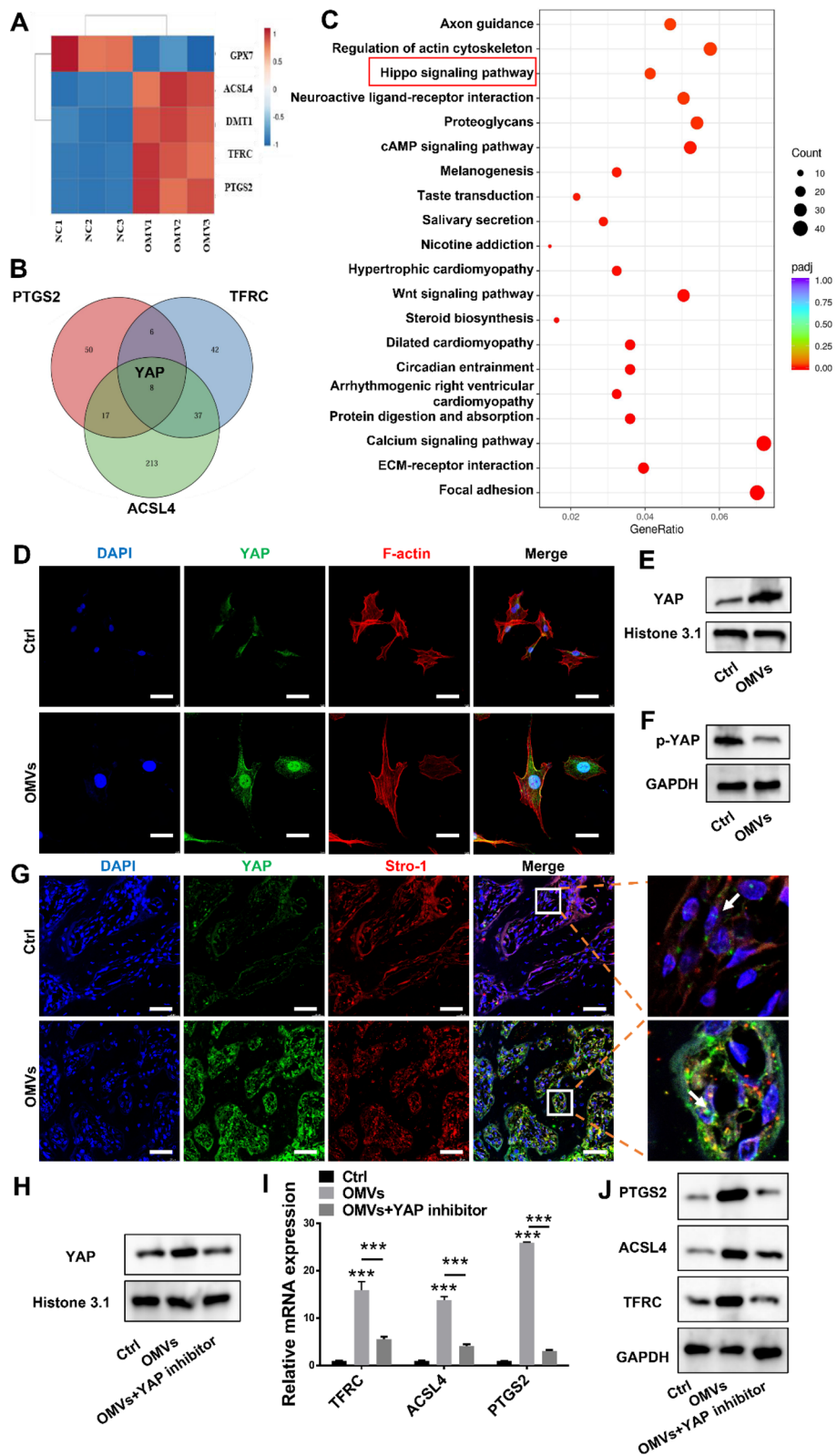


Fig. 8 (See legend on previous page.)

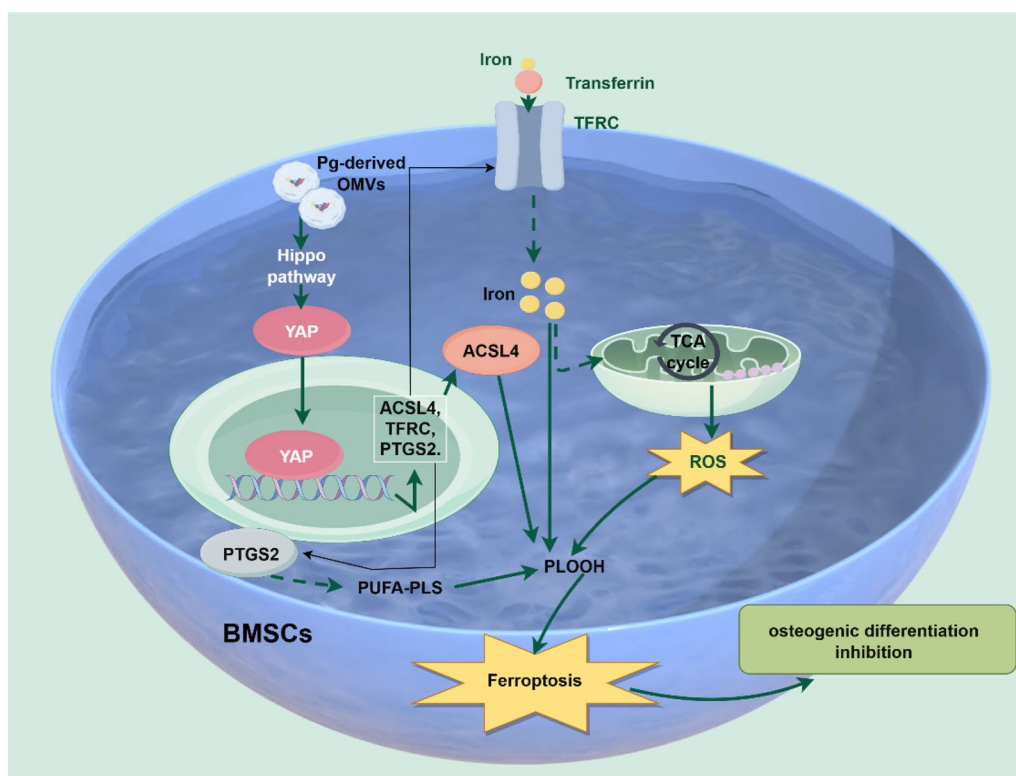


Fig. 9 Schematic diagram of the proposed molecular mechanism underlying Pg-derived OMVs inducing ferroptosis in BMSCs. Pg-derived OMVs mediated YAP nuclear translocation through the Hippo pathway, upregulating the expression of ACSL4, TFRC, and PTGS2 to promote ferroptosis

treat extraction sockets, and the results showed that Pg-derived OMVs significantly inhibited bone regeneration. In vitro, results revealed that Pg-derived OMVs inhibited the osteogenic differentiation of BMSCs.

To further investigate the specific mechanism for which Pg-derived OMVs were implicated in inhibiting BMSCs osteogenic differentiation, we performed RNA sequencing analysis, which revealed significant upregulation of ferroptosis in BMSCs treated with Pg-derived OMVs. Subsequent validation and rescue experiments results supported our finding that OMVs inhibit the osteogenic differentiation of BMSCs by mediating ferroptosis, thereby inhibiting bone regeneration in extraction sockets. Recently, bacteria-induced ferroptosis has become the focus of attention, but the specific virulence factors that induce such ferroptosis still need to be explored and elucidated. Previous study has reported that *Mycobacterial* can mediate ferroptosis in macrophages through tyrosine phosphatase A (PtpA) [39]. Besides, *Pseudomonas aeruginosa* was reported to induce ferroptosis in bronchial epithelium cells through lipoxygenase [40]. Our study confirmed for the first time that bacteria can induce ferroptosis by secreting OMVs, which is an essential finding of this study. Notably, the mechanism of Pg-derived OMVs inducing BMSCs ferroptosis

remains unknown. In our study, KEGG pathway analysis showed a significant down-regulation of the Hippo signaling pathway in Pg-derived-treated BMSCs, and nuclear expression of YAP was markedly increased in BMSCs treated with OMVs. YAP is known to be a key factor in promoting ferroptosis [32]. Thus, we speculated that Pg-derived OMVs may regulate BMSCs ferroptosis via YAP. To verify this hypothesis, a YAP inhibitor was used to reduce its expression. The results showed that inhibition of YAP expression in the OMVs-treated BMSCs significantly reduced the expression of ferroptosis markers (TFRC, ACSL4, and PTGS2). According to the above findings, our study confirmed that OMVs promoted ferroptosis in BMSCs via the Hippo-YAP pathway. Previous studies have established YAP's role in promoting ferroptosis. Wu et al. demonstrated that intercellular interaction enhanced cancer cell ferroptosis via the NF2-YAP pathway [32]. Similarly, YAP-mediated ferroptosis has been implicated in the pathogenesis of primary ovarian insufficiency [41]. Additionally, the stiff substrate was reported to induce ferroptosis through YAP mediating mechanotransduction in the nucleus pulposus cell [42]. Our current results align consistently with these reported studies. However, YAP does not always induce ferroptosis. It has been reported that YAP can activate SLC7A11

through ATF4, increasing intracellular GSH to inhibit ferroptosis [43]. This may be related to the cell type and the microenvironment in which the cell is located.

Fer-1, a synthetic ferroptosis inhibitor, impedes ferroptosis by diminishing intracellular free Fe²⁺ and lipid peroxidation, which is consistent with the experimental results of the Fer-1 group in this study. Recently, targeting ferroptosis is an important means to promote osteogenesis and treat osteoporosis. A study has reported that curcumin-containing DNA tetrahedron-based could target ferroptosis to treat diabetic osteoporosis [44]. Another research has shown that the delivery of ferroptosis inhibitor by hydrogel composite 3D-printed could promote the repair of infected bone defects [45]. These materials have potential applications in promoting bone regeneration under dysregulation of periodontitis microflora in the future, and more targeting ferroptosis delivery systems can be designed to facilitate bone regeneration under dysregulation of periodontitis.

Conclusion

In conclusion, our study indicates that Pg microbiota imbalance inhibits bone regeneration by secreting OMVs. Mechanistically, we confirmed that Pg-derived OMVs inhibited bone regeneration by inducing BMSCs ferroptosis via the Hippo-YAP pathway. Furthermore, targeting ferroptosis significantly rescued the poor bone regeneration of extraction sockets caused by Pg-derived OMVs. These findings might provide a new insight and promising therapeutic target for promoting bone regeneration under oral microbiota imbalance.

Supplementary Information

The online version contains supplementary material available at <https://doi.org/10.1186/s12951-025-03457-0>.

Supplementary Material 1.

Acknowledgements

Graphical Abstract and Schematic diagram were created with Figdraw.

Author contributions

Conceptualization: X.L., Y.W., Q.L., S.C., X.Z., Y.C., X.Z., D.M.; Writing—original draft preparation: X.L.; Designing—figures and table: X.L., Y.W., T.N., S.T. D.M.; writing—review and editing: X.L., H.C., S.C., X.Z. D.M.; supervision: X.L., T.N., S.C., X.Z., Y.C., D.M.; funding acquisition: X.L., D.M. All authors have read and agreed to the published version of the manuscript.

Funding

This study was supported by National Natural Science Foundation of China (82470963), Scientific research. Science research cultivation program of stomatological hospital, southern medical university (PY2023027), and Guangzhou Municipal Basic and Applied Basic Research Project Funding by Science and Technology Projects in Guangzhou (2024A04J6614).

Data availability

The data that support the findings of this study are available from the corresponding author upon reasonable request.

Declarations

Ethics approval and consent to participate

The animal ethics approval was approved by the Nanfang Hospital Ethic Committee, Southern Medical University (Approval number IACUC-LAC-20230218-001). The human ethics approval by Ethics Committee of Stomatology Hospital of Southern Medical University (Approved number NYKQ-EC- [2024] 07).

Competing interests

The authors declare no competing interests.

Author details

¹Department of Endodontics, Stomatological Hospital, School of Stomatology, Southern Medical University, No. 366 Jiangnan Avenue South, Guangzhou 510280, Guangdong, China. ²Stomatological Hospital, School of Stomatology, Southern Medical University, No. 366 Jiangnan Avenue South, Guangzhou 510280, Guangdong, China. ³Department of Pediatric Dentistry, Stomatological Hospital, School of Stomatology, Southern Medical University, No 366 Jiangnan Avenue South, Guangzhou 510280, Guangdong, China.

Received: 26 December 2024 Accepted: 7 May 2025

Published online: 17 May 2025

References

- Deo PN, Deshmukh R. Oral microbiome: unveiling the fundamentals. *J Oral Maxillofac Pathol.* 2019;23:122–8.
- Banack HR, Genco RJ, LaMonte MJ, Millen AE, Buck MJ, Sun Y, et al. Cohort profile: the Buffalo OsteoPerio microbiome prospective cohort study. *BMJ Open.* 2018;8: e24263.
- Hascoët E, Blanchard F, Blin-Wakkach C, Guicheux J, Lesclous P, Cloitre A. New insights into inflammatory osteoclast precursors as therapeutic targets for rheumatoid arthritis and periodontitis. *Bone Res.* 2023;11:26.
- Yu B, Wang CY. Osteoporosis and periodontal diseases—an update on their association and mechanistic links. *Periodontol.* 2000;2022(89):99–113.
- Pihlstrom BL, Michalowicz BS, Johnson NW. Periodontal diseases. *Lancet.* 2005;366:1809–20.
- Díaz-Garrido N, Badia J, Baldomà L. Microbiota-derived extracellular vesicles in interkingdom communication in the gut. *J Extracell Vesicles.* 2021;10: e12161.
- González MF, Díaz P, Sandoval-Bórquez A, Herrera D, Quest A. *Helicobacter pylori* outer membrane vesicles and extracellular vesicles from *Helicobacter pylori*-infected cells in gastric disease development. *Int J Mol Sci.* 2021;22:4823.
- Hong M, Li Z, Liu H, Zheng S, Zhang F, Zhu J, et al. *Fusobacterium nucleatum* aggravates rheumatoid arthritis through FadA-containing outer membrane vesicles. *Cell Host Microbe.* 2023;31:798–810.
- Wang T, Mo L, Ou J, Fang Q, Wu H, Wu Y, et al. Proteus mirabilis vesicles induce mitochondrial apoptosis by regulating miR96-5p/Abca1 to inhibit osteoclastogenesis and bone loss. *Front Immunol.* 2022;13: 833040.
- Liu JH, Chen CY, Liu ZZ, Luo ZW, Rao SS, Jin L, et al. Extracellular vesicles from child gut microbiota enter into bone to preserve bone mass and strength. *Adv Sci.* 2021;8:2004831.
- Kim HY, Song MK, Gho YS, Kim HH, Choi BK. Extracellular vesicles derived from the periodontal pathogen *Filifactor alocis* induce systemic bone loss through Toll-like receptor 2. *J Extracell Vesicles.* 2021;10: e12157.
- Chen G, Sun Q, Cai Q, Zhou H. Outer membrane vesicles from *Fusobacterium nucleatum* switch M0-like macrophages toward the M1 phenotype to destroy periodontal tissues in mice. *Front Microbiol.* 2022;13: 815638.

13. Kim HY, Song MK, Lim Y, Jang JS, An SJ, Kim HH, et al. Effects of extracellular vesicles derived from oral bacteria on osteoclast differentiation and activation. *Sci Rep.* 2022;12:14239.
14. Zhang Z, Liu D, Liu S, Zhang S, Pan Y. The role of *Porphyromonas gingivalis* outer membrane vesicles in periodontal disease and related systemic diseases. *Front Cell Infect Microbiol.* 2020;10: 585917.
15. Farrugia C, Stafford GP, Murdoch C. *Porphyromonas gingivalis* outer membrane vesicles increase vascular permeability. *J Dent Res.* 2020;99:1494–501.
16. Dixon SJ, Lemberg KM, Lamprecht MR, Skouta R, Zaitsev EM, Gleason CE, et al. Ferroptosis: an iron-dependent form of nonapoptotic cell death. *Cell.* 2012;149:1060–72.
17. Jiang X, Stockwell BR, Conrad M. Ferroptosis: mechanisms, biology and role in disease. *Nat Rev Mol Cell Biol.* 2021;22:266–82.
18. Bersuker K, Hendricks JM, Li Z, Magtanong L, Ford B, Tang PH, et al. The CoQ oxidoreductase FSP1 acts parallel to GPX4 to inhibit ferroptosis. *Nature.* 2019;575:688–92.
19. Zhou Y, Zhou H, Hua L, Hou C, Jia Q, Chen J, et al. Verification of ferroptosis and pyroptosis and identification of PTGS2 as the hub gene in human coronary artery atherosclerosis. *Free Radic Biol Med.* 2021;171:55–68.
20. Li Y, Feng D, Wang Z, Zhao Y, Sun R, Tian D, et al. Ischemia-induced ACSL4 activation contributes to ferroptosis-mediated tissue injury in intestinal ischemia/reperfusion. *Cell Death Differ.* 2019;26:2284–99.
21. Lei G, Zhang Y, Koppula P, Liu X, Zhang J, Lin SH, et al. The role of ferroptosis in ionizing radiation-induced cell death and tumor suppression. *Cell Res.* 2020;30:146–62.
22. Yang Y, Lin Y, Wang M, Yuan K, Wang Q, Mu P, et al. Targeting ferroptosis suppresses osteocyte glucolipotoxicity and alleviates diabetic osteoporosis. *Bone Res.* 2022;10:26.
23. Maher P, Currais A, Schubert D. Using the oxytosis/ferroptosis pathway to understand and treat age-associated neurodegenerative diseases. *Cell Chem Biol.* 2020;27:1456–71.
24. Zhang C, Liu X, Jin S, Chen Y, Guo R. Ferroptosis in cancer therapy: a novel approach to reversing drug resistance. *Mol Cancer.* 2022;21:47.
25. Lu J, Yang J, Zheng Y, Chen X, Fang S. Extracellular vesicles from endothelial progenitor cells prevent steroid-induced osteoporosis by suppressing the ferroptotic pathway in mouse osteoblasts based on bioinformatics evidence. *Sci Rep.* 2019;9:16130.
26. Ma H, Wang X, Zhang W, Li H, Zhao W, Sun J, et al. Melatonin suppresses ferroptosis induced by high glucose via activation of the Nrf2/HO-1 signaling pathway in type 2 diabetic osteoporosis. *Oxid Med Cell Longev.* 2020;2020:9067610.
27. Wang X, Ma H, Sun J, Zheng T, Zhao P, Li H, et al. Mitochondrial ferritin deficiency promotes osteoblastic ferroptosis via mitophagy in type 2 diabetic osteoporosis. *Biol Trace Elem Res.* 2022;200:298–307.
28. Luo X, Yin J, Miao S, Feng W, Ning T, Xu S, et al. mTORC1 promotes mineralization via p53 pathway. *Faseb J.* 2021;35: e21325.
29. Toyofuku M, Nomura N, Eberl L. Types and origins of bacterial membrane vesicles. *Nat Rev Microbiol.* 2019;17:13–24.
30. Miotto G, Rossetto M, Di Paolo ML, Orian L, Venerando R, Roveri A, et al. Insight into the mechanism of ferroptosis inhibition by ferrostatin-1. *Redox Biol.* 2020;28: 101328.
31. Zheng Y, Pan D. The hippo signaling pathway in development and disease. *Dev Cell.* 2019;50:264–82.
32. Wu J, Minikes AM, Gao M, Bian H, Li Y, Stockwell BR, et al. Intercellular interaction dictates cancer cell ferroptosis via NF2-YAP signalling. *Nature.* 2019;572:402–6.
33. Li W, Cao Y, Xu J, Wang Y, Li W, Wang Q, et al. YAP transcriptionally regulates COX-2 expression and GCCSystm-4 (G-4), a dual YAP/COX-2 inhibitor, overcomes drug resistance in colorectal cancer. *J Exp Clin Cancer Res.* 2017;36:144.
34. Hu W, Chen S, Zou X, Chen Y, Luo J, Zhong P, et al. Oral microbiome, periodontal disease and systemic bone-related diseases in the era of homeostatic medicine. *J Adv Res.* 2024. <https://doi.org/10.1016/j.jare.2024.08.019>.
35. Cheng X, Zhou X, Liu C, Xu X. Oral osteomicrobiology: the role of oral microbiota in alveolar bone homeostasis. *Front Cell Infect Microbiol.* 2021;11: 751503.
36. Li Q, Wang H, Liu L, Weng Y, Xu S, Li L, et al. Suppression of the NLRP3 inflammasome through activation of the transient receptor potential channel melastatin 2 promotes osteogenesis in tooth extraction sockets of periodontitis. *Am J Pathol.* 2023;193:213–32.
37. Ahn JJ, Shin HI. Bone tissue formation in extraction sockets from sites with advanced periodontal disease: a histomorphometric study in humans. *Int J Oral Maxillofac Implants.* 2008;23:1133–8.
38. Yin H, Chen CY, Liu YW, Tan YJ, Deng ZL, Yang F, et al. *Synechococcus elongatus* PCC7942 secretes extracellular vesicles to accelerate cutaneous wound healing by promoting angiogenesis. *Theranostics.* 2019;9:2678–93.
39. Qiang L, Zhang Y, Lei Z, Lu Z, Tan S, Ge P, et al. A mycobacterial effector promotes ferroptosis-dependent pathogenicity and dissemination. *Nat Commun.* 2023;14:1430.
40. Dar HH, Tyurina YY, Mikulska-Ruminska K, Shrivastava I, Ting HC, Tyurin VA, et al. *Pseudomonas aeruginosa* utilizes host polyunsaturated phosphatidylethanolamines to trigger theft-ferroptosis in bronchial epithelium. *J Clin Invest.* 2018;128:4639–53.
41. Wang F, Liu Y, Ni F, Jin J, Wu Y, Huang Y, et al. BNC1 deficiency-triggered ferroptosis through the NF2-YAP pathway induces primary ovarian insufficiency. *Nat Commun.* 2022;13:5871.
42. Ke W, Liao Z, Liang H, Tong B, Song Y, Li G, et al. Stiff substrate induces nucleus pulposus cell ferroptosis via YAP and N-cadherin mediated mechanotransduction. *Adv Healthc Mater.* 2023;12: e2300458.
43. Gao R, Kalathur R, Coto-Llerena M, Ercan C, Buechel D, Shuang S, et al. YAP/TAZ and ATF4 drive resistance to Sorafenib in hepatocellular carcinoma by preventing ferroptosis. *Embo Mol Med.* 2021;13: e14351.
44. Li Y, Cai Z, Ma W, Bai L, Luo E, Lin Y. A DNA tetrahedron-based ferroptosis-suppressing nanoparticle: superior delivery of curcumin and alleviation of diabetic osteoporosis. *Bone Res.* 2024;12:14.
45. Yuan K, Yang Y, Lin Y, Zhou F, Huang K, Yang S, et al. Targeting bacteria-induced ferroptosis of bone marrow mesenchymal stem cells to promote the repair of infected bone defects. *Adv Sci.* 2024;11: e2404453.

Publisher's Note

Springer Nature remains neutral with regard to jurisdictional claims in published maps and institutional affiliations.